Receptor for Hyaluronan-Mediated Motility (RHAMM) defines an invasive niche associated with tumor progression and predicts poor outcomes in breast cancer patients

Sarah E. Tarullo[1,2], Yuyu He[1,2], Claire Daughters[1,2], Todd P. Knutson[1,3], Christine M. Henzler[1,3], Matthew A. Price[1,2], Ryan Shanley[2], Patrice Witschen[1,2], Cornelia Tolg[4], Rachael E. Kaspar[1,2], Caroline Hallstrom[1], Lyubov Gittsovich[2], Megan L. Sulciner[5], Xihong Zhang[2,6], Colleen L. Forster[7], Carol A. Lange[2,6], Oleg Shats[8], Michelle Desler[8], Kenneth H. Cowan[8], Douglas Yee[2,6], Kathryn L. Schwertfeger[1,2], Eva A. Turley[4], James B. McCarthy[1,2], Andrew C. Nelson[1,2]

[1]Department of Laboratory Medicine and Pathology, University of Minnesota, Minneapolis, MN, USA

[2]Masonic Cancer Center, University of Minnesota, Minneapolis, MN, USA

[3]Minnesota Supercomputing Institute, University of Minnesota, Minneapolis, MN, USA

[4]London Health Sciences Center, Western University, Ontario, Canada

[5]School of Medicine, University of Minnesota, Minneapolis, MN, USA

[6]Department of Medicine, University of Minnesota, Minneapolis, MN, USA

[7]Clinical and Translational Science Institute, University of Minnesota, Minneapolis, MN, USA

[8]Eppley Institute for Research in Cancer, University of Nebraska Medical Center, Omaha, NE, USA

Abstract

Breast cancer invasion and metastasis result from a complex interplay between tumor cells and the tumor microenvironment (TME). Key oncogenic changes in the TME include aberrant synthesis,

processing and signaling of hyaluronan (HA). Hyaluronan Mediated Motility Receptor (RHAMM, *HMMR*) is an HA receptor enabling tumor cells to sense and respond to this aberrant TME during breast cancer progression. Previous studies have associated RHAMM expression to breast tumor progression, however cause and effect mechanisms are incompletely established. Focused gene expression analysis of an internal breast cancer patient cohort confirms increased *RHAMM* expression correlates with aggressive clinicopathological features. To probe mechanisms, we develop a novel 27-gene RHAMM-related signature (RRS) by intersecting differentially expressed genes in lymph node (LN) positive patient cases with the transcriptome of a RHAMM-dependent model of cell transformation, which we validate in an independent cohort. We demonstrate RRS predicts for poor survival and is enriched for cell cycle and TME-interaction pathways. Further analyses using CRISPR/Cas9 generated *RHAMM*–/– breast cancer cells provide direct evidence that RHAMM promotes invasion *in vitro* and *in vivo*. Immunohistochemistry studies highlight heterogeneous RHAMM protein expression, and spatial transcriptomics associates the RRS with RHAMM-high microanatomic foci. We conclude RHAMM upregulation leads to the formation of 'invasive niches', which are enriched in RRS-related pathways that drive invasion and could be targeted to limit invasive progression and improve patient outcomes.

Keywords

breast cancer; hyaluronan; extracellular matrix

INTRODUCTION

Despite improvements in screening and treatments, breast cancer remains the second leading cause of cancer-related deaths in women in the United States [1]. Breast cancer mortality is impacted by advanced stage disease at presentation and recurrence [2]. The capability of cancer cells to modify and infiltrate adjacent tissue is a hallmark common to all stages of breast cancer progression [3]. Mechanisms driving breast cancer invasion and metastasis are still poorly understood but involve an intricate interplay between tumor cells and various aspects of the tumor microenvironment (TME). A tumor-supportive TME is constructed in a complex manner that involves active remodeling of the extracellular matrix (ECM) [4]. A major ECM component utilized by tumor cells to create a supportive TME is the glycosaminoglycan hyaluronan (HA), which is actively metabolized by tumor and host stromal cells [5,6]. HA primarily exists as a high molecular weight polymer during homeostasis where fragmentation into low molecular weight (LMW) forms is tightly controlled [7]. HA fragments are generated during tissue stress and injury, and these are sensed as 'danger signals' by HA receptor combinations including CD44, LYVE1, TLR2,4, and RHAMM (Receptor for hyaluronan mediated motility) to initiate cell repair responses including motility and invasion [8–14]. This mechanism is normally dampened once tissues are repaired, but it is hijacked by tumors to maintain elevated HA production and fragmentation, which facilitates malignant progression [6,9].

Tumor-induced dysregulation of HA metabolism includes increased synthesis of high molecular weight (HMW) HA polymers by one or more hyaluronan synthases (HAS1-3). HA fragmentation is coupled to increased enzymatic- (hyaluronidase1 and 2, cell migration

inducing hyaluronidase 1) and chemically- (reactive oxygen species a.k.a. ROS) induced degradation of HMW-HA to LMW-HA and oligomers [9–16]. These LMW-HA fragments activate signaling pathways via HA receptors to support tumor cell proliferation, survival, invasion, and metastasis of many cancer types [6,17,18]. Specifically this aberrant HA metabolism in breast cancer is associated with tumor invasion and poor patient outcomes [19]. Depleting autocrine HA synthesis in tumor cells results in decreased tumorigenic potential and invasion, which emphasizes the importance of tumor cell-derived HA in malignant breast cancer progression [19]. CD44 and RHAMM are two HA receptors functionally associated with breast cancer progression and metastasis [19,20]. While CD44 is ubiquitously expressed [21], RHAMM (gene *HMMR*) expression is low under homeostatic conditions in most tissues including breast/mammary glands [22], but is upregulated in response to wound repair, inflammation and/or tumor formation [23–25]. Elevated RHAMM expression is associated with higher stage and/or poor outcome in several cancers, including breast cancer [26–31].

RHAMM was originally identified as a fibroblast motogenic protein [25,32], but has been further characterized as a multifunctional oncogenic protein that integrates a multitude of signaling networks to impact tumor cell metabolism, mitosis, cell motility, and invasion [33]. RHAMM is an intracellular protein that is unconventionally exported to the cell surface under stress conditions where it interacts with other co-receptors to regulate growth factor receptor (e.g. EGFR, PDGFR) and CD44 signaling [34]. At the cell surface RHAMM-CD44 interactions result in oncogenic signaling activated by LMW-HA [33,34]. Intracellular RHAMM is found in both the cytoplasm and nucleus. Cytoplasmic RHAMM associates with microtubule and vimentin cytoskeleton networks to form dynein motor complexes, which localize to the centrosome and maintain spindle integrity to promote cellular proliferation and motility [35–37]. Nuclear RHAMM forms transcriptional complexes with E2F1 to regulate the expression of genes such as fibronectin [38]. While the association of RHAMM expression with cancer is well documented, the precise pro-tumorigenic role(s) and mechanism(s) by which RHAMM promotes cancer progression remain poorly understood.

In the present study, we identify a gene expression signature that highlights mechanisms underlying the impact of RHAMM in primary invasive tumor expansion and lymph node (LN) metastasis of human breast cancers. We integrate differential gene expression from LN positive breast cancer patients with a cell model of RHAMM-driven transformation to develop a novel RHAMM Related Signature (RRS). We demonstrate that RRS associates with poor outcomes in an independent clinical cohort, highlighting the potential clinical importance of these RHAMM-related pathways. We show that RHAMM protein expression in breast tumors is heterogeneous with distinct regions enriched for strongly positive cells. These RHAMM-high foci are frequently observed near the invasive margin, and digital spatial transcriptomic analysis associates the RRS with these RHAMM-high regions. Our data further demonstrate a requirement for RHAMM expression in anchorage independent growth and invasion *in vitro* and invasive progression of *in vivo* intraductal xenografts using CRISPR/Cas9-generated deletion of *RHAMM* in breast tumor cell lines. We therefore conclude that high RHAMM expression in breast tumor cell subsets defines an 'invasive

niche' in breast cancer. We further propose that targeting critical elements within this niche will lead to improved therapies to limit malignant progression to improve patient outcomes.

MATERIALS AND METHODS

Cell Culture:

MCF10DCIS.com cell lines (provided by Dr. Fariba Behbod) were sub-cultured in Dulbecco's Modified Medium/Ham's Nutrient Mixture F-12 + %5 horse serum (Thermo Fisher Scientific, Waltham, MA, USA, Cat.# 51448C). MDA-MB-231 cells were cultured in DMEM supplemented with 10% Fetal Bovine Serum (Biotechne, Minneapolis, MN, USA, Cat.# S11550. Cells were regularly tested for mycoplasma and validated against STR profiles.

RHAMM CRISPR cell lines:

The human-codon-optimized Cas9 cDNA and chimaeric guide RNA (gRNA) were acquired from Addgene (41815 and 41824). Cas9 was PCR amplified and cloned into pENTR221 using SnaBI and XbaI sites engineered into the PCR primers. pENTR221 was then transferred to pT3.5-CAG-DEST by standard LR Clonase (Invitrogen) reaction, following the manufacturer's instructions. The chimaeric gRNA was PCR amplified and cloned into pENTR221 using SnaBI and XbaI. gRNAs targeting RHAMM were designed using Zfit software (http://zifit.partners.org/ZiFiT/). gRNAs targeting RHAMM were generated using inverse PCR of pENTR221-gRNA using Accuprime Pfx Supermix (Invitrogen), following the manufacturer's instructions. Purified PCR products were then treated with polynucleotide kinase and T4 Ligase (New England Biolabs), following the manufacturer's instructions. New gRNAs were sequence verified by standard Sanger sequencing. MCF10DCIS.com and MDA-MB-231 RHAMM KO cell lines were generated by transfection with paired guide RNA's, 5' GTATTGTATTTGATTAGAAT 3' and 5' GAATTTGAGAATTCTAAGCT 3' in plasmid pCR4-TOPO-U6-HPRT-gRNA. Guide RNA plasmids were co-transfected with the plasmid expressing the CAS9 enzyme (pT3.5 Caggs-FLAG-hCas9) as well as two plasmids for Puromycin and GFP selection, pcDNA-PB7 and pPBSB-CG-LUC-GFP(Puro)(+CRE). Transfection was performed using Lipofectamine LTX Reagent with PLUS Reagent (MCF10DCIS.com cell line, Invitrogen, Waltham, MA, Cat# 15338100) or UltraCruz transfection reagent (MDA-MB-231 cell line, Santa Cruz Biotechnology, Dallas, TX, Cat# sc-395739) following the manufacturers' protocols. Cells were plated clonally in 96 well plates 48 hours post-transfection in the presence of 0.6 μg/ml puromycin. Purified genomic DNA from the surviving clones was screened initially by genomic PCR to detect cell lines harboring the genomic deletion using the following primers: 5'AGATACTACCTTGCCTGCTTCA3' and 5'ACCTGCAGCTTCATCTCCAT3'. Clones were subsequently screened by western blot to evaluate the loss of RHAMM protein expression.

3D culture assays:

3D culture assays were performed as previously described [39]. Briefly Parental, Control, and RHAMM KO MCF10DCIS.com cell lines were imbedded in Matrigel (Corning, Corning, NY, USA, Cat.# 345234) plus 20% collagen type I (Corning, Corning, NY, USA,

Cat.# 354249) and 10 ug/mL low-molecular weight HA (R&D, Minneapolis, MN, USA Cat.#GLR001). Cells embedded in matrix were grown for 5–7 days, then fixed in 10% Neutral buffered formalin (NBF) for subsequent paraffin embedding and analysis.

MTT Proliferation Assay:

For each timepoint, MTT reagent (5mg/mL, Thermo Fisher Scientific, Waltham, MA, USA Cat.#: M6494,) was added to each well and incubated for 2 hours at 37°C protected from light. Solubilization buffer was added (95% DMSO in PBS) for 10 minutes followed by reading absorbance at 540 nm.

Immunofluorescence:

Cells were cultured in an 8 well chamber slide (Sigma Cat.#: C7057), fixed in 4% paraformaldehyde and where appropriate permeabilized with 0.2% TritonX-100. RHAMM and LaminB1 antibody (Supplemental Table 3) incubation was overnight at 4°C, then secondary (RHAMM:AlexaFluor 594, LaminB1:AlexaFluor 647) for 1 hour at room temperature (RT), and coverslipped with ProLong Gold Antifade DAPI (Invitrogen, Waltham, MA, USA Cat.# P36931). Slides were imaged on a Keyence BZ-X Series Microscope.

Anchorage Independent Colony Formation Assay:

Cells were cultured in 0.3% agarose solution for 21 days, with media changed every 3–4 days. Colonies (> 50 μM) were counted under an inverted light microscope.

Animal Model:

8–10 week old, female, NOD-*scid* IL2Rgamma^{null} mice (Jackson Laboratories) were injected intraductally (MIND model) as previously described [40]. Intraductal injection of 10,000 cells was performed bi-laterally into the #4 mammary gland. Tumors were measured bi-weekly using calipers, with volumes calculated using the formula length × width × width/0.5. Upon sacrifice, tumor-bearing mammary glands were measured via calipers and weighed prior to fixation and paraffin embedding.

Immunoblotting:

Cells were lysed in RIPA buffer with protease inhibitors (Roche, Cat#11836170001). Protein was quantified using a DC protein assay (BioRad, Cat#: 5000111). Equal amounts of protein were loaded on 8% SDS gels and transferred to PVDF membrane for immunoblotting. Antibody information is provided in Supplemental Table 3.

RT-qPCR:

RNA was harvested using TriPure Isolation reagent (Sigma, Cat#: 11667165001). cDNA was made using qScript cDNA synthesis kit (QuantaBio, Cat #101414-098). qPCR was performed using SYBR-green (VWR, Cat #101414-144) on a BioRad iQ5 Thermocycler. CD44 primers: Forward: 5' - GAT GGA GAA AGC TCT GAG CAT C -3' Reverse: 5' - TTG CTC CAC AGA TGG AGT TG -3'. RHAMM PrimePCR primers were obtained from BioRad (Cat#: 10025636).

Histology and Immunohistochemistry (IHC):

Breast cancer xenografts were collected, fixed with 10% NBF, and paraffin embedded. Two H&E-stained levels were analyzed by a pathologist (ACN) as previously described [39] to estimate the proportion of *in situ* (intraductal) xenograft tumor area compared to invasive tumor area across both levels. Categories were defined as the percentage of invasive tumor area to total tumor area as follows: 0 = 0% invasive area (intraductal tumor only); 1 = <20% invasive tumor area; 2 = 20%–80% invasive tumor area; and 3 = >80% invasive tumor area. The greatest linear dimension of invasive tumor was measured on histologic sections to determine pathologic tumor size consistent with standard clinical practice. IHC was performed to evaluate the expression of RHAMM, Ki67, and phospho-histone 3 (pH3). For HA-binding protein (HABP), rehydrated slides were divided into 2 sets: one incubated with a 1% hyaluronidase and one with TBST only at 37°C for 30 minutes, then TBST and blocked in Sniper blocking (Biocare Medical, Cat.# BS966) for one hour at RT. Anti-bHABP (Calbiochem) was applied to all slides and incubated overnight at 4°C, rinsed again, avidin-biotin-complex (ABC, Vector Labs) was applied for one hour at RT, rinsed, and counterstained with CATHematoxylin diluted 1:2 (Biocare Medical) for 5 minutes. Human breast cancer samples (n= 81) were stained for RHAMM (CD168) as above, and then scored by a pathologist (ACN). Antibody information is provided in Supplemental Table 3. Immunohistochemistry images were acquired on a Leica DM400B microscope (Wetzlar, Germany), at 20× or 40× objectives using a Leica DFC310 FX camera (Wetzlar, Germany) and LAS V3.8 software. Five images of at least 3 representative tumors were analyzed.

Digital Spatial Profiling:

A formalin-fixed paraffin-embedded (FFPE) section was prepared using the GeoMx DSP RNA Slide Prep Kit for FFPE, in-situ hybridized using GeoMx Cancer Transcriptome Atlas (CTA) probe set and stained using the GeoMx Morphology Kit for (NanoString, Seattle WA) which distinguishes tumor/epithelial cells (cytokeratin+), immune cells (CD45+) and other cell types (dsDNA+/cytokeratin-/CD45-). Regions of interest (ROIs) were selected by a pathologist (ACN) in conjunction with a serial section IHC stained for RHAMM to comprise at least 75% cytokeratin positive cells. Paired ROIs were selected for statistical replication, and each ROI pair was annotated by the microanatomical location (tumor margin vs. tumor core) and RHAMM stain intensity (low vs. high). Cleaved probes were sequenced and raw read counts uploaded to the GeoMx DSP Control Center (Version 2.3.0.268) for quality control (QC), scaling, and normalization. QC flagged ROIs and probes were excluded from downstream analysis. The raw read counts were scaled based on the ratio of the geometric mean ROI area to the measured surface area of each ROI and normalized to the 3rd quartile of all selected probes.

NanoString nCounter Gene Expression Analysis:

A custom gene set (n=356) was developed covering genes involved in TME interactions, inflammatory signaling, steroid receptor and growth factor signaling, cell cycle, apoptosis, and DNA repair, plus PAM50 classifier genes. Raw gene expression counts were analyzed within R (ver 3.6.1, R Core Team, 2019) using the NanoStringQCPro package (ver 1.18.0). Flagged outliers (26 cases out of 120 cases) were removed for downstream analysis. After

normalization, each gene was median-centered and scaled (root mean square) based on expression levels across all 94 high-quality samples.

Microarray Gene Expression Analysis:

Raw microarray expression data from the Breast Cancer Collaborative Registry (BCCR) [41] was exported from Feature Extraction software (ver 7.5.1, Agilent Technologies) and analyzed within R using the limma package (ver 3.42.2). Major outliers (n = 20) were removed, leaving 656 samples for downstream analysis. Probes were removed from the dataset if they were not annotated with a gene symbol or were not expressed above background levels in most samples, leaving 24,625 probes included in downstream analyses. Gene expression alterations driven by RHAMM overexpression were explored via microarray analysis of RHAMM-transfected cells (LR21) and parental 10T1/2 cells. Methods and data of this experiment were published by Tolg et. al. [42], with differential gene expression data included in Supplemental Data 1.

Gene Expression Plotting:

Data were explored by hierarchal clustering of median-centered and scaled gene expression values by calculating a Pearson correlation distance matrix and linked using the Ward1 (ward.D) algorithm in R. Heatmaps were generated using the aheatmap function from the NMF R package (ver 0.23.0). Boxplots were generated by in R that describe the median, hinges correspond to the 1st and 3rd quartiles, and the whisker extends from each hinge 1.5 * IQR.

HA Fragmentation Analysis:

Analysis of HA fragmentation was performed as previously described [43] using concentrated cell culture conditioned medium.

Flow cytometry:

Cells were harvested via scraping, filtered through a 40 μM filter and blocked via FcR (FACS) buffer. Cells were stained using Zombie NIR™ fixable viability kit and CD44 (Supplemental Table 3). Flow cytometry was performed on Cytek Aurora machine. Flow cytometric events were defined by forward and side scatter, doublet discrimination, and viable cells. Cells were then gated on minus debris and singlets. Data analysis was performed with FlowJo.v10.7.2

HA binding assay:

Cells were harvested using Accutase (BioLegend, CA, USA, Cat.# 423201,) and filtered through a 40 μm strainer. Preexisting HA matrices were removed via hyaluronidase (2.5 mg/mL, MilliporeSigma, MD, USA, Cat # H3506) treatment for 30 min at 37°C. Cells were stained for viability using Zombie NIR™ fixable viability kit for 15 min at room temperature (BioLegend, CA, USA, Cat.# 423105), followed by fluorescently labeled low-molecular weight HA (2.5mg/ml in PBS) for 1 hour at room temperature. Flow cytometry was performed on a BD LSR Fortessa H0081 machine. Data analysis was performed with FlowJo.v10.7.2.

HA internalization assay:

Cells were incubated with TexasRed labeled LMW HA (Cat #H-025R, Echelon Biosciences) in fresh medium for 45 min at 37 °C in dark, then washed with PBS and fixed with 2% PFA. Cells were subsequently permeabilized with 2% Triton X-100 for 30 minutes, stained with Phalloidin (1:500 dilution, Thermo Fisher Scientific, MA, USA, Cat # 501720934,) for 1 hour at RT, and mounted with ProLong™ gold antifade with DAPI (Invitrogen, OR, USA, Cat.# P36931). Images were acquired on a on a Leica DM400B microscope (Wetzlar, Germany) at 400X.

Statistics:

All in vitro studies were performed in biological triplicates, unless otherwise noted. All animal studies were repeated at least twice with representative data shown. Quantitative experiment values are shown as mean and standard deviations, unless otherwise noted. Survival curves were plotted by Kaplan Meier method and the difference between curves was evaluated by a log-rank test. Differences of the distribution of categorical variables were evaluated by Chi-square test or Fisher's exact test (when the expected frequency < 5). Differences in quantitative values among experimental groups were evaluated by t-test or one-way ANOVA (with Tukey's post-hoc test). Logistic regression was performed to estimate odds ratio and coefficients of categorical dummy variables. $P < 0.05$ was considered statistically significant. All data visualization and statistical analysis were performed using R version 3.6.1 or GraphPad Prism version 8.0.0. TCGA analysis was performed using UCSC Xena Browser [44].

Study approval:

The UMN cohort (IRB Approval Study# 1409E53504) was collected from archived pathology tissue blocks with de-identified clinical data; all participants had agreed to the institution's standard consent for research participation. The BCCR cohort was collected as previously described [41]. All animal studies were approved by the IACUC of the University of Minnesota, protocol number 1810–36470.

RESULTS

RHAMM expression is correlated with clinicopathological features of aggressive breast cancers

We first explored transcriptional regulation of pathways related to TME interactions, immune milieu, oncogenic signaling, and PAM50 gene expression in a retrospective patient cohort of human breast cancer (n=94) from the University of Minnesota (UMN) Medical Center using a custom Nanostring gene expression probe set (GSE224883). We found increased RHAMM transcript level significantly associated with LN metastasis (Figure 1A), higher Nottingham tumor grade (Figure 1B), and more aggressive breast cancer subtypes by both PAM50 molecular classification (Figure 1C) and clinical hormone receptor expression (Figure 1D). This result is consistent with a role for RHAMM function in breast cancer progression.

To better understand the molecular mechanism(s) of RHAMM in breast cancer progression we identified the top 50 differentially expressed genes between LN+ versus LN− patients from the UMN patient cohort. To specifically identify RHAMM-related oncogenic molecular mechanisms, we also utilized differentially expressed genes (Supplemental Data File 1) from a C57BL/6 murine model wherein overexpression of an oncogenic Rhamm isoform increased cell motility, *in vivo* tumor engraftment, and metastasis [42,45]. Intersection of these two gene sets produced a 27-gene RHAMM-related signature (RRS) (Supplemental Table 1) highlighting potential biological consequences of RHAMM activation and signaling in primary human breast cancers demonstrating clinically significant invasive progression. Pathway enrichment analysis [46,47] of the RRS showed significant association with cell cycle-related pathways including: E2F1 targets, G2-M checkpoint, mitotic spindle regulation, and MYC targets. Also enriched were genes associated with ECM-receptor interactions, focal adhesion, and epithelial-mesenchymal transition pathways (Supplemental Table 2). Hierarchical clustering analysis of the UMN patient cohort with RRS genes resulted in RRS-high and RRS-low subsets (Figure 1E). Like RHAMM univariate expression, the RRS-high cluster was significantly enriched for cases with higher Nottingham tumor grade (Supplemental Figure 1A), LN metastasis (Supplemental Figure 1B), and more aggressive PAM50 subtypes (Supplemental Figure 1C). We then assessed the association of either elevated RHAMM expression or RRS-high status with larger invasive tumor size (as defined by clinical pT stage). We found that patients with larger invasive primary tumors have significantly higher odds ratio (OR) to have high RHAMM (Figure 1F, OR=2.8) and RRS (Figure 1G, OR=4.2). Overall, these data indicate that increased RHAMM expression associates with regulation of proliferation, motility, and ECM interactions that correlate with larger invasive primary tumor growth and regional LN metastasis.

Immunohistochemical (IHC) staining for RHAMM protein was then performed to confirm the biologic significance of RHAMM transcript analyses and characterize the spatial distribution of RHAMM expression in the complex TME. RHAMM protein expression was greatest in breast tumor cells but varied both by the proportion of positive cells and the stain intensity within individual cells (Figure 2A&B). H-scores [48,49] quantified by a pathologist to summarize heterogeneous RHAMM protein expression showed significant agreement with transcript levels across the cohort (R = 0.66, p = 2.6e-11, Supplemental Figure 2). RHAMM H-scores also trend with increased LN metastasis (Figure 2C), are significantly associated with higher Nottingham tumor grade (Figure 2D), and aggressive breast cancer subtypes (Figure 2E, 2F) similar to *RHAMM* transcript levels. Importantly, we noted focally enriched RHAMM expression in distinct areas of the invasive tumor margin in triple negative, high grade ER+, and HER2+ breast cancer cases (Supplemental Figure 3). We therefore performed digital spatial profiling using the 1800-gene Cancer Transcriptome Atlas probe set on a representative case of high-grade, triple-negative breast cancer that showed heterogenous RHAMM expression with higher RHAMM protein expression at the tumor margin compared to the tumor core (Figure 2 G–I). Hierarchical clustering of regions of interest (ROIs) from the core and margin with the RRS demonstrated enrichment of this signature at the RHAMM-high tumor margin (Figure 2J). These data suggest that focal enrichment of RHAMM+ tumor cells at the tumor margin are linked to pathways associated

with RHAMM activation and positively correlate with breast cancer progression to larger invasive tumor sizes and potentially LN metastasis.

RHAMM drives breast cancer invasion

To directly identify how RHAMM contributes to invasive breast cancer progression, we generated RHAMM KO cell lines using CRISPR/Cas9 technology in MCF10DCIS.com cells, a transformed, hormone-receptor negative mammary epithelial cell line which is an established model for studying mechanisms of tissue invasion [40]. This model was chosen in part because preliminary analysis showed moderate to high *RHAMM* transcript expression compared to other common human breast cancer cell lines (Supplemental Data File 2). Immunoblot analysis confirms complete loss of RHAMM protein expression in two independent KO lines (Figure 3A, Supplemental Figure 4A). Although RHAMM can associate with CD44, RT-PCR and flow cytometry analysis demonstrated that CD44 expression or surface localization were not altered by RHAMM-loss (Figure 3B, Supplemental Figure 4B). Immunofluorescence staining comparing permeabilized and unpermeabilized cells in parental and control cells demonstrates RHAMM expression in a cytoplasmic/cell membrane pattern and on mitotic spindles and confirms complete loss of RHAMM expression in KO cells (Figure 3C, Supplemental Figure 5). RHAMM loss did not significantly affect tumor cell production of HA nor alter HA fragmentation in culture (Supplemental Figure 4C&D). Further, cell surface binding and cell internalization of exogenous LMW-HA added to the culture medium were not altered by RHAMM loss (Supplemental Figure 4E&F). Collectively, these data demonstrate that stable knockout of RHAMM does not significantly perturb CD44 expression or HA metabolism *in vitro*.

We next assessed the effects of RHAMM KO on breast cancer invasion phenotypes *in vitro*. Proliferation in standard two-dimensional culture was not significantly impacted by RHAMM KO (Figure 4A). Conversely, RHAMM loss significantly decreases tumor cell ability to grow in anchorage independent conditions (Figure 4B). In 3D Matrigel cultures, RHAMM KO significantly decreases the percentage of colonies with an invasive growth pattern compared to control and parental cells (Figure 4C). Finally, vimentin protein expression, a biomarker associated with mesenchymal plasticity and motility [50], was consistently decreased in MCF10DCIS.com RHAMM KO cells (Figure 4D). The same CRISPR/Cas9 strategy was used to knockout *RHAMM* in MDA-MB-231 cells (Figure 4E, Supplemental Figure 6), an additional triple negative breast cancer cell line. Similar to what was observed with the MCF10DCIS.com cells, we observed that RHAMM KO did not alter MDA-MB-231 cell proliferation but did impair cell growth in anchorage independent conditions (Figure 4F&G). We also observe a significant decrease in RHAMM KO cell invasion in a transwell invasion assay (Figure 4H). Taken together, these data show RHAMM promotes breast tumor cell invasion and anchorage independent growth.

To directly assess RHAMM KO in a complex TME, we performed *in vivo* studies using the mouse mammary intraductal (MIND) model which enables study of mechanisms that promote invasive tumor growth in an orthotopic TME [40,51]. We injected parental, control, and RHAMM KO1 MCF10DCIS.com cells into the ducts of the fourth mammary gland of NSG mice. After approximately 4 weeks, wildtype xenografts undergo reliable

expansion into palpable tumors (Figure 5A). At an endpoint of six weeks, many parental and control tumors reached maximum allowable tumor volume (2000 mm^3) while all animals injected with RHAMM KO1 cells survived with minimal grossly appreciable tumor burden (Supplemental Figure 7A). Subsequent histologic analysis of the proportion of intraductal to invasive tumor growth reveals the majority of parental (75%) and mock control (93%) tumors show nearly complete progression to an invasive tumor (>80% of tumor area) (Figure 5B). Conversely, 0% of RHAMM KO tumors demonstrated this extent of invasive progression, and the majority (50%) never progressed beyond pure intraductal proliferation compared to 16.7% and 0% in parental and control tumors, respectively. RHAMM KO tumors that demonstrated invasive growth had significantly smaller maximum invasive tumor sizes (Figure 5C) and correspondingly lower gross tumor volume volumes and weights (Supplemental Figure 7B&C).

Further IHC analysis of wildtype tumors reveal a significant increase in the percentage of RHAMM-positive tumor cells in invasive areas when compared to intraductal areas in wildtype parental and control tumors (Figure 5D), indicating a spontaneous upregulation of RHAMM during invasive progression in this model. Quantification of Ki67 showed no significant differences in Ki67+ cells between parental, control, and KO tumors in either *in situ* (Supplemental Figure 7D) or invasive tumors (Supplemental Figure 7E), indicating that genomic *RHAMM* deletion did not cause a quiescent tumor cell phenotype *in vivo*. However, assessment of the mitotic-phase marker phosphorylated histone H3 (pH3) [52–55] shows significant differences in the average number of pH3+ cells per 10 high power fields in the invasive areas of *RHAMM* wildtype controls compared to invasive KO xenografts (Supplemental Figure 7F), indicating RHAMM may promote more frequent mitotic cell division *in vivo*. HA, measured by HABP [56], accumulates at the leading edge of invasive tumors, variably within the tumor core, and at the periphery of DCIS lesions (Figure 5E, Supplemental Figure 7G&H). Interestingly, we observed higher intra-tumoral HA accumulation in invasive components of RHAMM KO tumors (Figure 5E), which may suggest more complex alterations in HA metabolism with loss of RHAMM *in vivo* which were not detected *in vitro*. Overall, these data demonstrate that RHAMM expression is required for breast tumor cell invasion.

RHAMM Related Signature (RRS) correlates with poor outcomes in breast cancer patients

To validate the clinical significance of our findings we analyzed microarray expression data from the Breast Cancer Collaborative Registry (BCCR) at the University of Nebraska. Corroborating our previous results (Figure 1E), unsupervised hierarchical clustering of the BCCR dataset also identifies RRS high patients who are enriched for aggressive clinicopathological features (Figure 6A, Supplemental Figure 8A–C). Importantly, RRS-high patients have worse 10-year overall survival than RRS-low patients in this independent patient cohort (Figure 6B). The integration of RHAMM and downstream/associated pathways in the RRS provides superior prognostic separation of this patient cohort than *RHAMM* transcript expression alone (Figure 6C). Additional analysis using the TCGA breast cancer dataset also corroborates that RRS predicts for worse overall survival (Figure 6D), than *RHAMM* expression alone (Figure 6E). Overall, our findings define RHAMM as a key mediator of breast cancer progression. We propose a novel gene expression signature,

RRS, which may identify aggressive breast cancers with increased potential for tissue invasion and worse overall survival.

DISCUSSION

Tissue invasion and metastasis are a unified hallmark of cancer [57] and the capacity for tumor cell invasive motility is an irrevocable feature of metastasis [3]. Increased RHAMM expression has been previously linked to breast cancer progression [26,58], but the specific downstream effectors of increased RHAMM in breast tumor cells have not previously been fully elucidated. RHAMM functions in multiple cellular compartments, including interactions with the mitotic spindle [59], cytoplasmic interphase microtubules [37], nuclear transcriptional regulators [38] and with HA and CD44 at the cell surface [60,61]; this diversity complicates understanding which functions are most critical to invasive progression.

It is notable that RHAMM expression within the tumor parenchyma is not uniform but rather is detected within discrete regions at the leading tumor margin in areas of active ECM remodeling. Furthermore, the RRS expression pattern comprises both cell cycle and ECM-interactions, which are enriched in RHAMM-high versus RHAMM-low regions of the same tumor. While correlative, these observations collectively suggest localized RHAMM expression and/or HA-mediated RHAMM activation may define specific remodeling 'invasive niches' that efficiently support proliferation, invasive motility, and tumor expansion.

Both *RHAMM* expression and the RRS-high phenotype were strongly associated with larger primary tumor size in patients, consistent with RHAMM supporting rapid growth and invasive progression in our MIND xenograft model. Despite the relationship between elevated *RHAMM* expression and RRS-high signatures on patient tumor size, there was no apparent difference in the expression of Ki67 in parental/control versus RHAMM KO xenograft tumors in the MCF10DCIS.com model, notwithstanding the well-recognized use of Ki67 expression as a clinical proliferation marker. However parental/control xenograft tumors demonstrated a higher G2/M tumor fraction compared to RHAMM KO tumors as indicated by increased levels of pH3 staining. This leads us to conclude that RHAMM may specifically support efficient completion of the cell cycle in the complex *in vivo* TME to drive invasive expansion. This conclusion is consistent with a prior study linking RHAMM interactions with Aurora kinase-A at centrosomes to promote a phenotype of enhanced cell cycle-dependent engraftment and motility associated with poor prognosis in breast cancer [62]. Association of the RRS with decreased overall survival in patients suggest that RHAMM oncogenic activities corresponding to cell cycle may be clinically informative. Diagnostically, combining RHAMM protein expression with a marker of elevated *in vivo* mitotic fraction, such as pH3, may be a straightforward method to identify these more aggressive cancers.

In addition to cell cycle regulation, there is substantial evidence indicating that interactions between tumor cells and their microenvironment are critically important for driving invasion and malignant progression. Since RHAMM is dynamically regulated in the context of cell

stress, it is well positioned to enable cells to sense and respond the remodeling ECM by detecting changes in HA metabolism within the TME [9,63]. Accordingly, multiple genes in the RRS are linked to ECM-interactions, cell adhesion, and EMT suggesting that increased RHAMM expression in patient tumors may be critically important for sensing localized remodeling within expanding tumors [64]. Studies have shown that RHAMM may functionally associate with another HA receptor, CD44, to coordinate tumor cellular responses to extracellular HA with nuanced functional cooperativity and redundancy [60,65]. For example, previous work has shown treatment of cells with anti-RHAMM blocking antibodies modulates CD44 expression in an extracellular HA concentration-dependent manner [60]. In our MCF10DCIS.com model, CD44 levels are equivalent between wildtype and RHAMM-KO *in vitro*; however, our results contrast to other reports linking RHAMM and CD44 expression [60]. These differences may reflect variables in distinct cell culture methods, including HA concentrations, or may be due to intrinsic cell line differences. Separately, Nedvetzki et al. have shown increased accumulation of HA substrate is associated with functional compensation for CD44-knockout without significantly changing total RHAMM expression [65]. Of note, our KO xenograft tumors that develop limited invasive growth show qualitatively strong HA staining, suggesting a potential compensatory mechanism of increased extracellular HA inducing a CD44-dependent response. Future work should address the mechanism(s) activated by RHAMM:HA interaction during breast cancer cell invasion, define the dependency of these mechanisms on co-function with CD44, and assess the utilization of specific *RHAMM* isoforms, which may differently impact oncogenic activities [66].

One limitation of this study and the development of the RRS is that the human expression data in both cohorts was generated with probes that do not distinguish between *RHAMM* isoforms. In contrast, the initial murine model of Rhamm-driven transformation used to develop the RRS is based on a unique murine isoform smaller than full length which maintains the HA- and centrosome-binding domains [42,45]. Future studies in human breast cancer cohorts that can distinguish full-length *RHAMM* (NM_001142556.2, 725 aa) and delta-exon 4 *RHAMM* (NM_012485.3, 709 aa) [66] will be necessary to disambiguate the contributions of these distinct isoforms to breast cancer progression and to further clarify the downstream pathways activated in association with each isoform. A second limitation of this study is the utilization of the MCF10DCIS.com xenograft model. This model was chosen not only for the moderate/high levels of RHAMM expression, but also for their ability to respond to TME signals to progress from *in situ* to invasive tumors [67]. However, this ability to respond to paracrine signals may explain some discrepancies in our *in vitro* and *in vivo* data, specifically the differences observed in invasion in our control MCF10DCIS.com cells. It is likely we observe these differences due to subtle yet complex differences in the cells ability to sense and respond to local growth factors present in the *in vitro* and then more dynamic *in vivo* environment. Another limitation of the MCF10DCIS.com xenograft model is that it generally does not metastasize. While we observe a significant decrease in invasion in RHAMM KO tumors, which is an obligate precursor for metastasis [3], we acknowledge this could be due to lead time difference, as all mice were sacrificed at six weeks. Additional metastatic xenograft models are necessary to further confirm the necessity

of RHAMM in invasive progression and mechanisms involved in the later stages of the metastatic cascade.

While elevated RHAMM is clearly related to increased malignant progression, the current studies emphasize the complexities associated with this involvement. Elevated RHAMM levels and corresponding RRS emphasize that RHAMM impacts multiple oncogenic pathways. These pathways are linked to altered cell growth and tumor cell interactions with the actively remodeling TME. Identifying key structural domains within RHAMM and expression and activity of different RHAMM isoforms will lead to mechanistic insights on how RHAMM integrates into these complex pro-tumorigenic pathways and provide new opportunities for improving patient diagnosis and treatment.

Supplementary Material

Refer to Web version on PubMed Central for supplementary material.

ACKNOWLEDGEMENTS

DATA AVAILABILITY STATEMENT

The data that support the findings of this study are available at Gene Expression Omnibus database (GSE224883) at the time of publication or available within manuscript and/or supplementary materials.

REFERENCES

1. Siegel RL, Miller KD, Fuchs HE, et al. Cancer statistics, 2022. CA Cancer J Clin 2022; 72: 7–33. [PubMed: 35020204]

2. Feng Y, Spezia M, Huang S, et al. Breast cancer development and progression: Risk factors, cancer stem cells, signaling pathways, genomics, and molecular pathogenesis. Genes Dis 2018; 5: 77–106. [PubMed: 30258937]

3. Welch DR, Hurst DR. Defining the Hallmarks of Metastasis. Cancer Res 2019; 79: 3011–3027. [PubMed: 31053634]

4. Winkler J, Abisoye-Ogunniyan A, Metcalf KJ, et al. Concepts of extracellular matrix remodelling in tumour progression and metastasis. Nat Commun 2020; 11: 5120. [PubMed: 33037194]

5. Chanmee T, Ontong P, Itano N. Hyaluronan: A modulator of the tumor microenvironment. Cancer Lett 2016; 375: 20–30. [PubMed: 26921785]

6. Caon I, Bartolini B, Parnigoni A, et al. Revisiting the hallmarks of cancer: The role of hyaluronan. Semin Cancer Biol 2020; 62: 9–19. [PubMed: 31319162]

7. Tavianatou AG, Caon I, Franchi M, et al. Hyaluronan: molecular size-dependent signaling and biological functions in inflammation and cancer. FEBS J 2019; 286: 2883–2908. [PubMed: 30724463]

8. Triggs-Raine B, Natowicz MR. Biology of hyaluronan: Insights from genetic disorders of hyaluronan metabolism. World J Biol Chem 2015; 6: 110–120. [PubMed: 26322170]

9. Tolg C, McCarthy JB, Yazdani A, et al. Hyaluronan and RHAMM in wound repair and the "cancerization" of stromal tissues. Biomed Res Int 2014; 2014: 103923. [PubMed: 25157350]

10. Skandalis SS, Karalis T, Heldin P. Intracellular hyaluronan: Importance for cellular functions. Semin Cancer Biol 2020; 62: 20–30. [PubMed: 31276783]

11. Turley EA, Noble PW, Bourguignon LY. Signaling properties of hyaluronan receptors. J Biol Chem 2002; 277: 4589–4592. [PubMed: 11717317]

12. Avenoso A, Bruschetta G, A DA, et al. Hyaluronan Fragmentation During Inflammatory Pathologies: A Signal that Empowers Tissue Damage. Mini Rev Med Chem 2020; 20: 54–65. [PubMed: 31490750]

13. Jackson DG. Hyaluronan in the lymphatics: The key role of the hyaluronan receptor LYVE-1 in leucocyte trafficking. Matrix Biol 2019; 78–79: 219–235.

14. Tammi MI, Oikari S, Pasonen-Seppanen S, et al. Activated hyaluronan metabolism in the tumor matrix - Causes and consequences. Matrix Biol 2019; 78–79: 147–164.

15. Pratt RL. Hyaluronan and the Fascial Frontier. Int J Mol Sci 2021; 22.

16. Weigel PH. Planning, evaluating and vetting receptor signaling studies to assess hyaluronan size-dependence and specificity. Glycobiology 2017; 27: 796–799. [PubMed: 28633290]

17. Wu W, Chen L, Wang Y, et al. Hyaluronic acid predicts poor prognosis in breast cancer patients: A protocol for systematic review and meta analysis. Medicine (Baltimore) 2020; 99: e20438. [PubMed: 32481447]

18. Auvinen P, Tammi R, Parkkinen J, et al. Hyaluronan in peritumoral stroma and malignant cells associates with breast cancer spreading and predicts survival. Am J Pathol 2000; 156: 529–536. [PubMed: 10666382]

19. Schwertfeger KL, Cowman MK, Telmer PG, et al. Hyaluronan, Inflammation, and Breast Cancer Progression. Front Immunol 2015; 6: 236. [PubMed: 26106384]

20. Jiang D, Liang J, Noble PW. Hyaluronan as an immune regulator in human diseases. Physiol Rev 2011; 91: 221–264. [PubMed: 21248167]

21. Yu S, Cai X, Wu C, et al. Adhesion glycoprotein CD44 functions as an upstream regulator of a network connecting ERK, AKT and Hippo-YAP pathways in cancer progression. Oncotarget 2015; 6: 2951–2965. [PubMed: 25605020]

22. Tolg C, Yuan H, Flynn SM, et al. Hyaluronan modulates growth factor induced mammary gland branching in a size dependent manner. Matrix Biol 2017; 63: 117–132. [PubMed: 28232112]

23. Greiner J, Ringhoffer M, Taniguchi M, et al. Receptor for hyaluronan acid-mediated motility (RHAMM) is a new immunogenic leukemia-associated antigen in acute and chronic myeloid leukemia. Exp Hematol 2002; 30: 1029–1035. [PubMed: 12225794]

24. Telmer PG, Tolg C, McCarthy JB, et al. How does a protein with dual mitotic spindle and extracellular matrix receptor functions affect tumor susceptibility and progression? Commun Integr Biol 2011; 4: 182–185. [PubMed: 21655434]

25. Turley EA. Purification of a hyaluronate-binding protein fraction that modifies cell social behavior. Biochem Biophys Res Commun 1982; 108: 1016–1024. [PubMed: 6185115]

26. Assmann V, Gillett CE, Poulsom R, et al. The pattern of expression of the microtubule-binding protein RHAMM/IHABP in mammary carcinoma suggests a role in the invasive behaviour of tumour cells. J Pathol 2001; 195: 191–196. [PubMed: 11592098]

27. Yamada Y, Itano N, Narimatsu H, et al. Receptor for hyaluronan-mediated motility and CD44 expressions in colon cancer assessed by quantitative analysis using real-time reverse transcriptase-polymerase chain reaction. Jpn J Cancer Res 1999; 90: 987–992. [PubMed: 10551329]

28. Li H, Guo L, Li JW, et al. Expression of hyaluronan receptors CD44 and RHAMM in stomach cancers: relevance with tumor progression. Int J Oncol 2000; 17: 927–932. [PubMed: 11029494]

29. Rein DT, Roehrig K, Schondorf T, et al. Expression of the hyaluronan receptor RHAMM in endometrial carcinomas suggests a role in tumour progression and metastasis. J Cancer Res Clin Oncol 2003; 129: 161–164. [PubMed: 12712331]

30. Rizzardi AE, Rosener NK, Koopmeiners JS, et al. Evaluation of protein biomarkers of prostate cancer aggressiveness. BMC Cancer 2014; 14: 244. [PubMed: 24708576]

31. Abetamann V, Kern HF, Elsasser HP. Differential expression of the hyaluronan receptors CD44 and RHAMM in human pancreatic cancer cells. Clin Cancer Res 1996; 2: 1607–1618. [PubMed: 9816340]

32. Hardwick C, Hoare K, Owens R, et al. Molecular cloning of a novel hyaluronan receptor that mediates tumor cell motility. J Cell Biol 1992; 117: 1343–1350. [PubMed: 1376732]

33. Messam BJ, Tolg C, McCarthy JB, et al. RHAMM Is a Multifunctional Protein That Regulates Cancer Progression. Int J Mol Sci 2021; 22.

34. Maxwell CA, McCarthy J, Turley E. Cell-surface and mitotic-spindle RHAMM: moonlighting or dual oncogenic functions? J Cell Sci 2008; 121: 925–932. [PubMed: 18354082]

35. Hatano H, Shigeishi H, Kudo Y, et al. RHAMM/ERK interaction induces proliferative activities of cementifying fibroma cells through a mechanism based on the CD44-EGFR. Lab Invest 2011; 91: 379–391. [PubMed: 20956971]

36. Wang Z, Wu Y, Wang H, et al. Interplay of mevalonate and Hippo pathways regulates RHAMM transcription via YAP to modulate breast cancer cell motility. Proc Natl Acad Sci U S A 2014; 111: E89–98. [PubMed: 24367099]

37. Assmann V, Jenkinson D, Marshall JF, et al. The intracellular hyaluronan receptor RHAMM/IHABP interacts with microtubules and actin filaments. J Cell Sci 1999; 112 (Pt 22): 3943–3954. [PubMed: 10547355]

38. Meier C, Spitschak A, Abshagen K, et al. Association of RHAMM with E2F1 promotes tumour cell extravasation by transcriptional up-regulation of fibronectin. J Pathol 2014; 234: 351–364. [PubMed: 25042645]

39. Tarullo SE, Hill RC, Hansen KC, et al. Postpartum breast cancer progression is driven by semaphorin 7a-mediated invasion and survival. Oncogene 2020; 39: 2772–2785. [PubMed: 32020054]

40. Kittrell F, Valdez K, Elsarraj H, et al. Mouse Mammary Intraductal (MIND) Method for Transplantation of Patient Derived Primary DCIS Cells and Cell Lines. Bio Protoc 2016; 6.

41. Sherman S, Shats O, Fleissner E, et al. Multicenter breast cancer collaborative registry. Cancer Inform 2011; 10: 217–226. [PubMed: 21918596]

42. Tolg C, Hamilton SR, Zalinska E, et al. A RHAMM mimetic peptide blocks hyaluronan signaling and reduces inflammation and fibrogenesis in excisional skin wounds. Am J Pathol 2012; 181: 1250–1270. [PubMed: 22889846]

43. Bhilocha S, Amin R, Pandya M, et al. Agarose and polyacrylamide gel electrophoresis methods for molecular mass analysis of 5- to 500-kDa hyaluronan. Anal Biochem 2011; 417: 41–49. [PubMed: 21684248]

44. Goldman MJ, Craft B, Hastie M, et al. Visualizing and interpreting cancer genomics data via the Xena platform. Nat Biotechnol 2020; 38: 675–678. [PubMed: 32444850]

45. Hall CL, Yang B, Yang X, et al. Overexpression of the hyaluronan receptor RHAMM is transforming and is also required for H-ras transformation. Cell 1995; 82: 19–26. [PubMed: 7541721]

46. Chen EY, Tan CM, Kou Y, et al. Enrichr: interactive and collaborative HTML5 gene list enrichment analysis tool. BMC Bioinformatics 2013; 14: 128. [PubMed: 23586463]

47. Kuleshov MV, Jones MR, Rouillard AD, et al. Enrichr: a comprehensive gene set enrichment analysis web server 2016 update. Nucleic Acids Res 2016; 44: W90–97. [PubMed: 27141961]

48. McCarty KS Jr., Miller LS, Cox EB, et al. Estrogen receptor analyses. Correlation of biochemical and immunohistochemical methods using monoclonal antireceptor antibodies. Arch Pathol Lab Med 1985; 109: 716–721. [PubMed: 3893381]

49. Fedchenko N, Reifenrath J. Different approaches for interpretation and reporting of immunohistochemistry analysis results in the bone tissue - a review. Diagn Pathol 2014; 9: 221. [PubMed: 25432701]

50. Thiery JP. Epithelial-mesenchymal transitions in tumour progression. Nat Rev Cancer 2002; 2: 442–454. [PubMed: 12189386]

51. Valdez KE, Fan F, Smith W, et al. Human primary ductal carcinoma in situ (DCIS) subtype-specific pathology is preserved in a mouse intraductal (MIND) xenograft model. J Pathol 2011; 225: 565–573. [PubMed: 22025213]

52. Crosio C, Fimia GM, Loury R, et al. Mitotic phosphorylation of histone H3: spatio-temporal regulation by mammalian Aurora kinases. Mol Cell Biol 2002; 22: 874–885. [PubMed: 11784863]

53. Goto H, Tomono Y, Ajiro K, et al. Identification of a novel phosphorylation site on histone H3 coupled with mitotic chromosome condensation. J Biol Chem 1999; 274: 25543–25549. [PubMed: 10464286]

54. Hendzel MJ, Wei Y, Mancini MA, et al. Mitosis-specific phosphorylation of histone H3 initiates primarily within pericentromeric heterochromatin during G2 and spreads in an ordered fashion coincident with mitotic chromosome condensation. Chromosoma 1997; 106: 348–360. [PubMed: 9362543]

55. Preuss U, Landsberg G, Scheidtmann KH. Novel mitosis-specific phosphorylation of histone H3 at Thr11 mediated by Dlk/ZIP kinase. Nucleic Acids Res 2003; 31: 878–885. [PubMed: 12560483]

56. de la Motte CA, Drazba JA. Viewing hyaluronan: imaging contributes to imagining new roles for this amazing matrix polymer. J Histochem Cytochem 2011; 59: 252–257. [PubMed: 21378279]

57. Hanahan D, Weinberg RA. The hallmarks of cancer. Cell 2000; 100: 57–70. [PubMed: 10647931]

58. Wang C, Thor AD, Moore DH 2nd, et al. The overexpression of RHAMM, a hyaluronan-binding protein that regulates ras signaling, correlates with overexpression of mitogen-activated protein kinase and is a significant parameter in breast cancer progression. Clin Cancer Res 1998; 4: 567–576. [PubMed: 9533523]

59. Chen H, Mohan P, Jiang J, et al. Spatial regulation of Aurora A activity during mitotic spindle assembly requires RHAMM to correctly localize TPX2. Cell Cycle 2014; 13: 2248–2261. [PubMed: 24875404]

60. Carvalho AM, Soares da Costa D, Reis RL, et al. RHAMM expression tunes the response of breast cancer cell lines to hyaluronan. Acta Biomater 2022; 146: 187–196. [PubMed: 35577044]

61. Carvalho AM, Soares da Costa D, Paulo PMR, et al. Co-localization and crosstalk between CD44 and RHAMM depend on hyaluronan presentation. Acta Biomater 2021; 119: 114–124. [PubMed: 33091625]

62. Chu TLH, Connell M, Zhou L, et al. Cell Cycle-Dependent Tumor Engraftment and Migration Are Enabled by Aurora-A. Mol Cancer Res 2018; 16: 16–31. [PubMed: 28993511]

63. Sohr S, Engeland K. RHAMM is differentially expressed in the cell cycle and downregulated by the tumor suppressor p53. Cell Cycle 2008; 7: 3448–3460. [PubMed: 18971636]

64. McCarthy JB, El-Ashry D, Turley EA. Hyaluronan, Cancer-Associated Fibroblasts and the Tumor Microenvironment in Malignant Progression. Front Cell Dev Biol 2018; 6: 48. [PubMed: 29868579]

65. Nedvetzki S, Gonen E, Assayag N, et al. RHAMM, a receptor for hyaluronan-mediated motility, compensates for CD44 in inflamed CD44-knockout mice: a different interpretation of redundancy. Proc Natl Acad Sci U S A 2004; 101: 18081–18086. [PubMed: 15596723]

66. Choi S, Wang D, Chen X, et al. Function and clinical relevance of RHAMM isoforms in pancreatic tumor progression. Mol Cancer 2019; 18: 92. [PubMed: 31072393]

67. Hu M, Yao J, Carroll DK, et al. Regulation of in situ to invasive breast carcinoma transition. Cancer Cell 2008; 13: 394–406. [PubMed: 18455123]
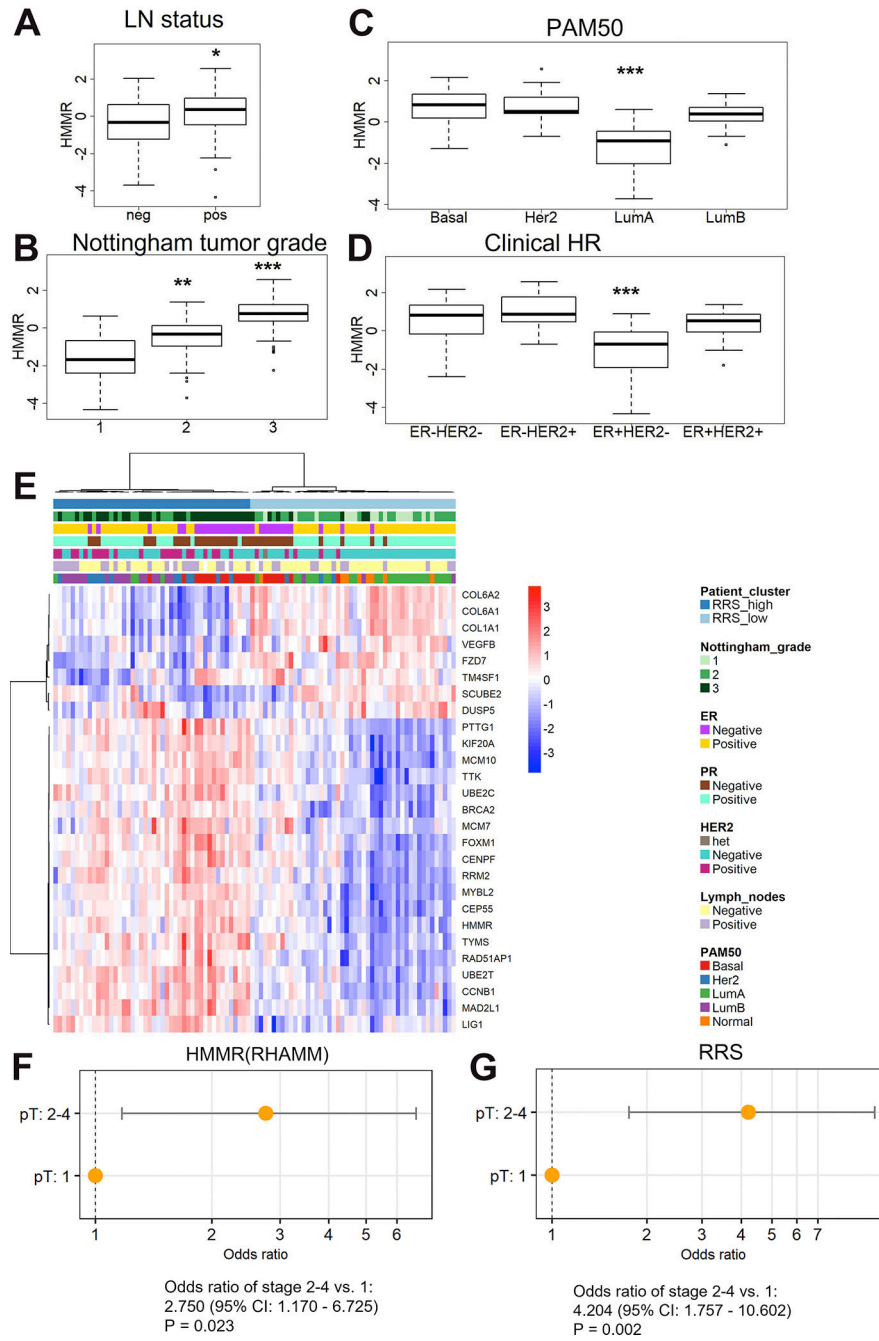
Figure 1. RHAMM expression is correlated with clinicopathological features of aggressive breast cancers.

Human breast cancer tissues from the UMN breast cancer cohort were analyzed by Nanostring gene expression. Levels of HMMR mRNA were increased in association with: (**A**) lymph node (LN) positive status, (**B**) increased Nottingham tumor grade, (**C**) basal, HER2-enriched, and Luminal B subtypes by PAM50, and (**D**) triple negative and HER2+ disease by clinical hormone receptor expression. (**E**) Unsupervised hierarchical clustering of 94 human breast cancer cases with a 27-gene signature of RHAMM biologic activity enriches for more aggressive disease features. (**F**) Logistic regression analysis of T-stage of

RHAMM high vs low patients. (**G**) Logistic regression analysis of T-stage of RRS high vs low patients. * = p<0.05, ** = p<0.01, *** = p<0.005. 1
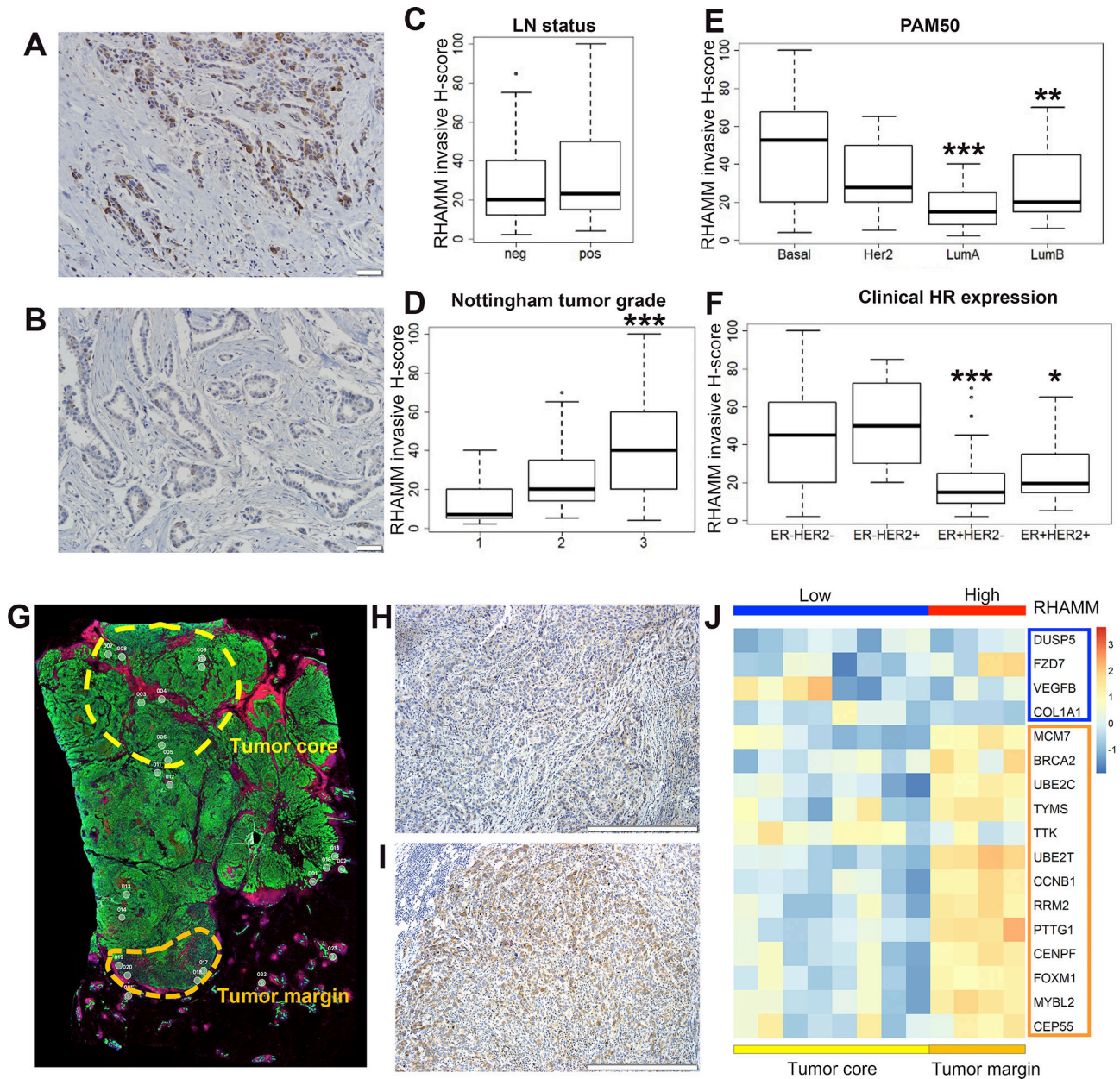
Figure 2. RHAMM protein and RRS expression is heterogeneous across patient samples but correlates with aggressive breast cancer s.

Representative RHAMM high (**A**) and low (**B**) expressing tissues, scale bars 50 μm. (**C-F**) RHAMM IHC were analyzed with high RHAMM levels correlating with: (**C**) lymph node (LN) positive status, (**D**) increased Nottingham tumor grade, (**E**) basal, HER2-enriched, and Luminal B subtypes by PAM50, and **F.** triple negative and HER2+ disease by clinical hormone receptor expression. (**G**) Overview image of a TNBC tumor stained for pan-cytokeratin (green), CD45 (red), and dsDNA (blue). Regions of interest (ROIs) are numbered 1–23 with those in the tumor margin or tumor core highlighted. Serial sections of tumor in panel (**G**) stained for RHAMM at the tumor core (**H**) or the tumor margin, scale bar

500 μm (**I**). (**J**) Modified RRS using ROIs located at the tumor core or tumor margin. * = p<0.05, ** = p<0.01, *** = p<0.005.
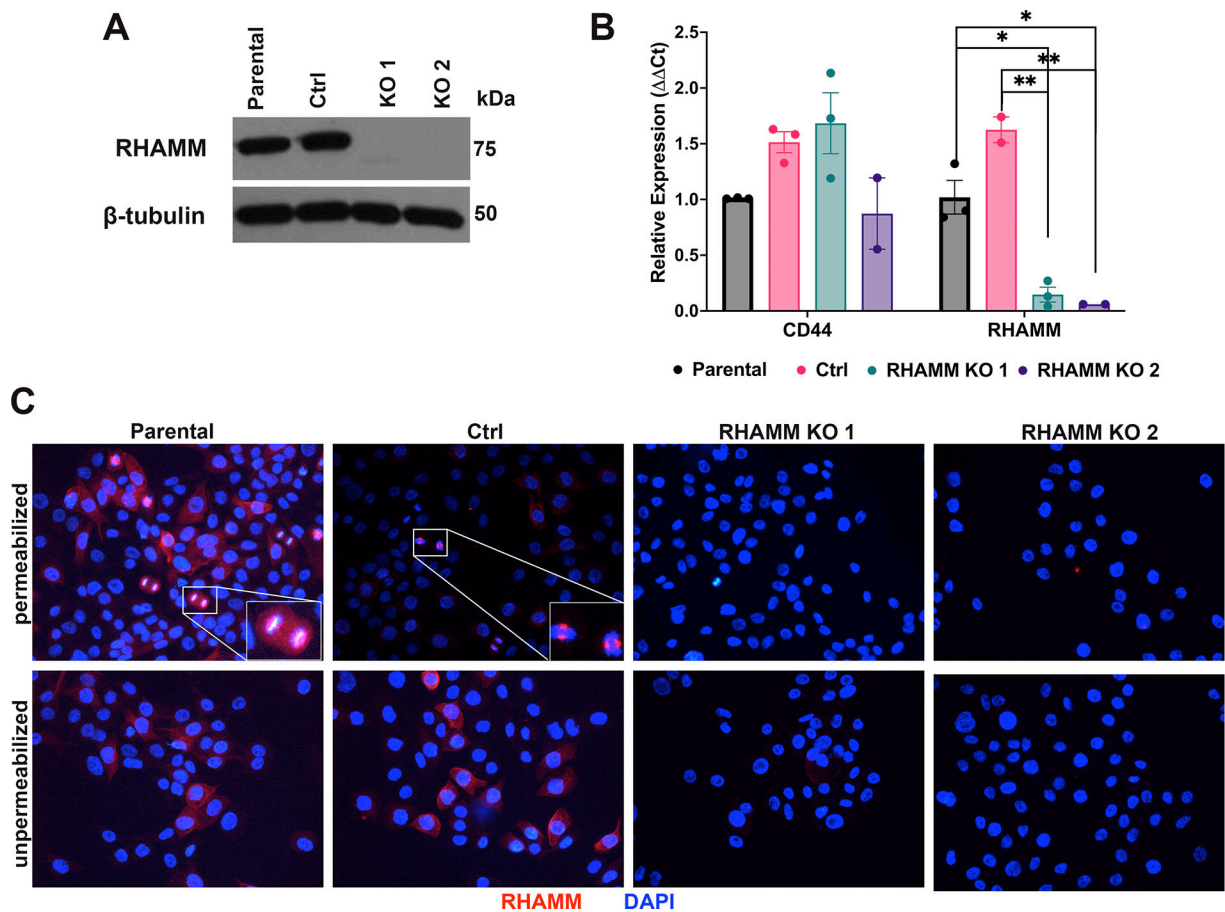
Figure 3. Characterization of RHAMM KO breast cancer cells.
(**A**) Representative immunoblot of MCF10DCIS.com parental, Ctrl, and RHAMM KO cell lines for RHAMM. (**B**) Quantitative-PCR expression of CD44 and RHAMM in MCF10DCIS.com parental, control and RHAMM KO cell lines. (**C**) Representative RHAMM immunofluorescence images of MCF10DCIS.com parental, control and RHAMM KO cell lines, in permeabilized and unpermeabilized conditions, insets highlighting mitotic spindle RHAMM staining. * = $p < 0.05$, ** = $p < 0.01$.
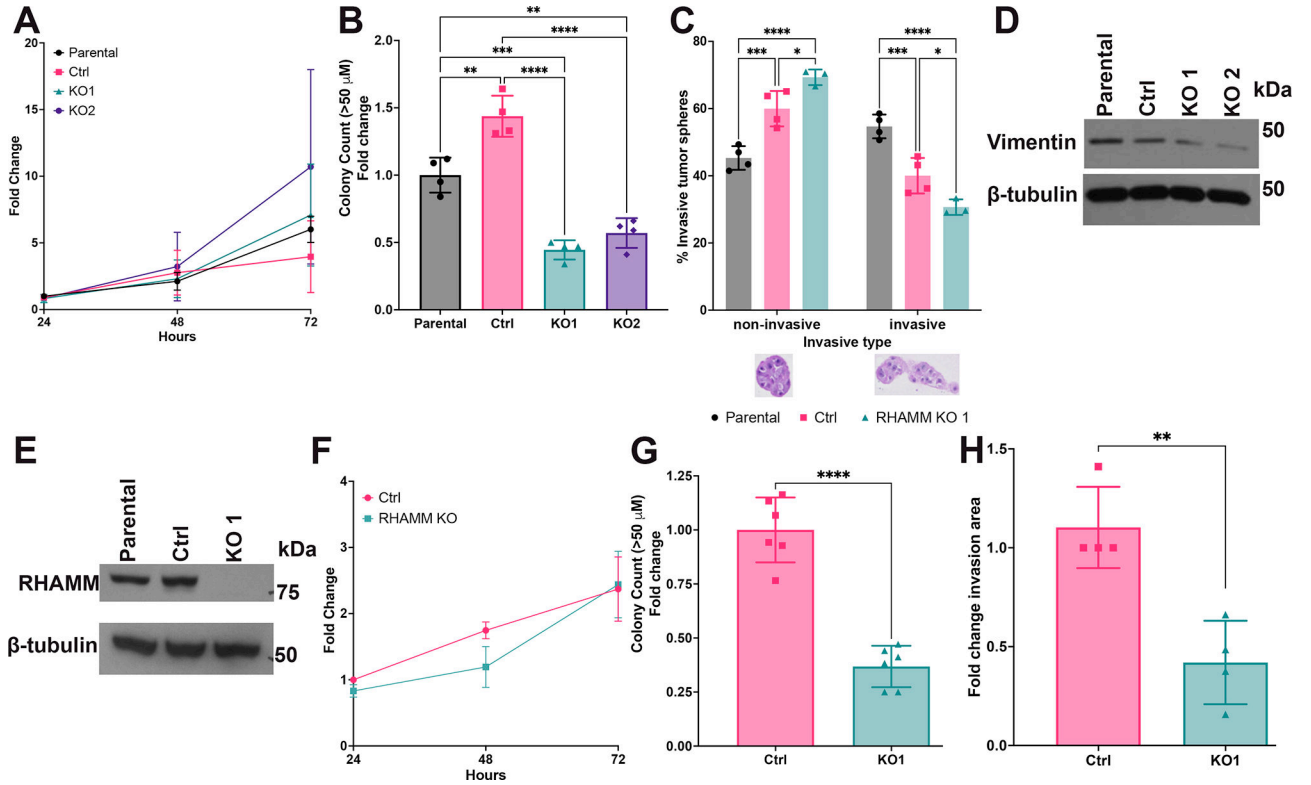
Figure 4. RHAMM drives phenotypes associated with invasive breast cancer in MCF10DCIS (A-D) and MDA-MB-231 cell lines (E-H).

MTT proliferation assay of (**A**) MCF10DCIS.com or (**F**) MDA-MB-231 parental, control and RHAMM KO cell lines. Colony counts (size >50μm) of (**B**) MCF10DCIS.com or (**G**) MDA-MB-231 parental, control and RHAMM KO cell lines in soft agar. (**C**) MCF10DCIS.com parental, control and RHAMM KO cell lines embedded in Matrigel + 20% collagen + 10 ug/mL LMW-HA and scored for invasion, representative images of tumor spheres below. (**D**) Representative immunoblot of vimentin in MCF10DCIS.com parental, control and RHAMM KO cell lines. (**E**) Representative immunoblot of MDA-MB-231 Ctrl and RHAMM KO cell lines for RHAMM. (**H**) Quantification of transwell migration assay of MDA-MB-231 control (Ctrl) and RHAMM KO cells. * = p<0.05, ** = p<0.01, *** = p<0.005, **** = p<0.001.
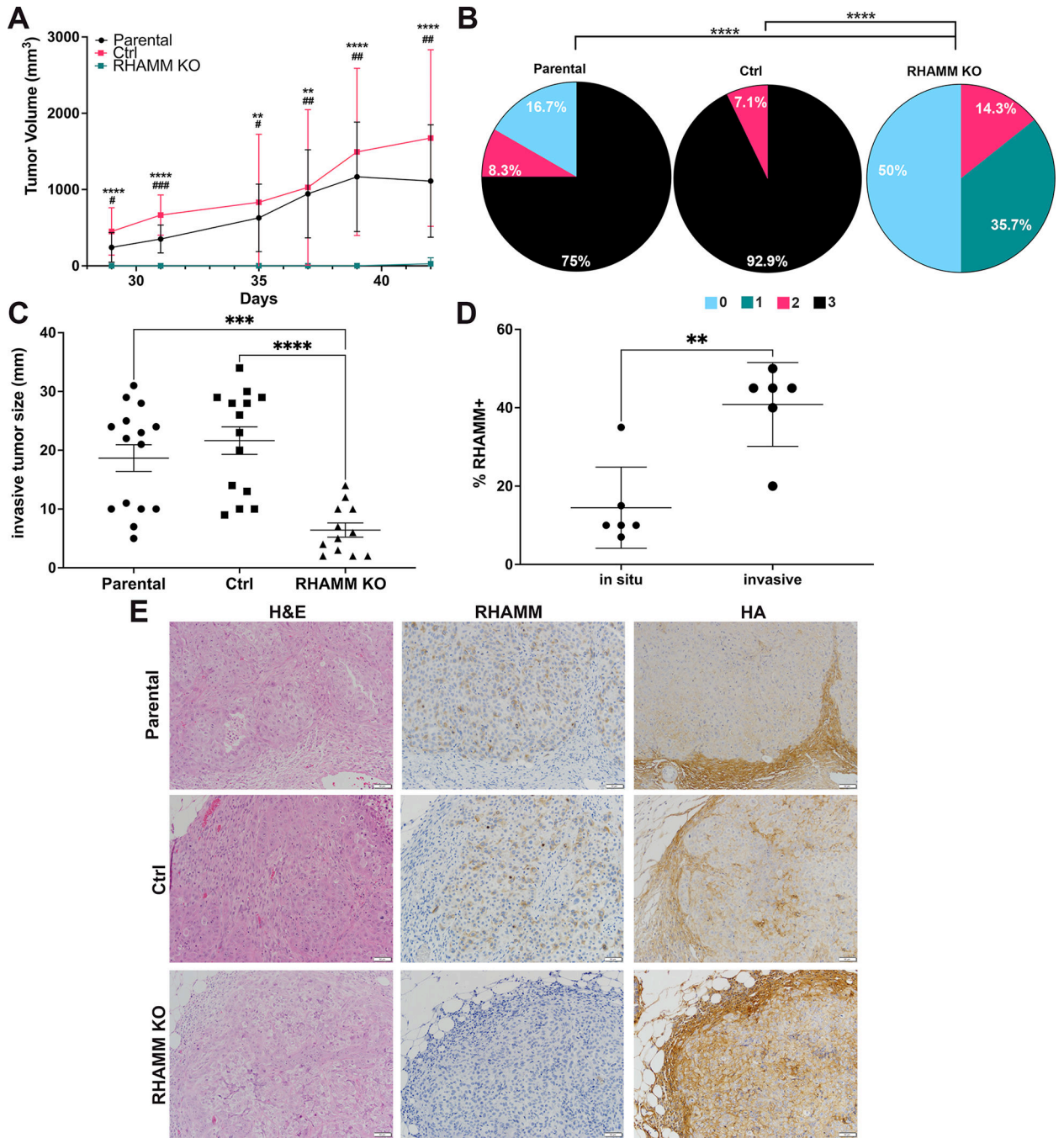
Figure 5. RHAMM drives breast tumor invasion.
(**A**) Tumor volumes for mice injected with MCF10DCIS.com parental, control (Ctrl), and RHAMM KO cells, * T-test Parental vs KO, # T-tests Ctrl vs KO. (**B**) Tumors from MCF10DCIS.com parental, control and RHAMM KO groups scored for proportion of invasive tumor area; 0 = intraductal tumor only; 1 = <20% invasive tumor area; 2 = 20–80% invasive tumor area; 3 = >80% invasive tumor area. (**C**) Size of invasive tumors from parental, control, and RHAMM KO cell lines. (**D**) MCF10DCIS.com parental tumors scored for invasion and then stained by IHC and scored for RHAMM expression (**E**) Representative

images of invasive tumors stained for H&E and IHC for RHAMM and HA, scale bars 100 μm. ** = p<0.01, *** = p<0.005, **** = p<0.001.
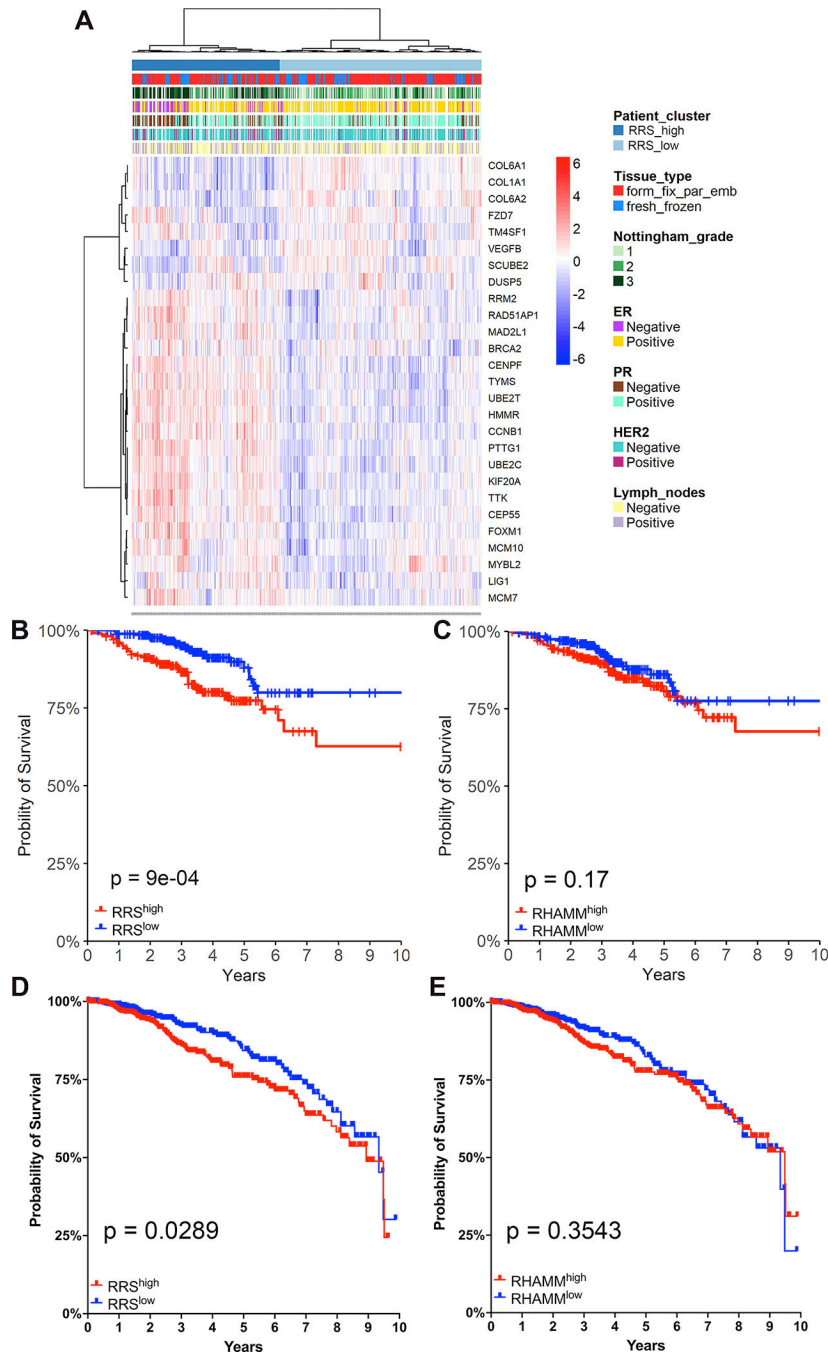
Figure 6. RRS correlates with poor outcomes in breast cancer patients
(**A**) Unsupervised hierarchical clustering of human breast cancer cases from the University of Nebraska breast cancer Collaborative Registry (BCCR). Kaplan-Meier plot of BCCR cases by RRS (**B**) or RHAMM (**C**) high or low for overall survival at 10 years. Kaplan-Meier plot of TCGA breast cancer cases by RRS (**D**) or RHAMM (**E**) high or low for overall survival at 10 years.